Electronic Charge Distributions for Heavy Ions at High Velocities*

HARRY H. HECKMAN, EDWARD L. HUBBARD, AND WILLIAM G. SIMON
Lawrence Radiation Laboratory, University of California, Berkeley, California
(Received 8 August 1962)

The equilibrium electronic charge-state distributions of C^{12}, N^{14}, O^{16}, and Ne^{20} ions in Zapon at energies between 1.59 and 10.5 MeV/nucleon are measured. The nonequilibrium charge distributions for Ar^{40} ions at 10.2 MeV/nucleon are also given. The experimental technique used makes possible measurements of charge states that comprise less than 10^{-5} of the total beam. The equilibrium charge data are satisfactorily interpreted by, and lend support to, the phenomenological theory of Dmitriev. It is found possible to present the ratio of loss to capture cross sections for the $1K$, $2K$, and $1L$ electrons and the mean ionic charge for all ions in terms of universal functions involving the ion velocity and ionic and nuclear charge. The relative values of the absolute cross sections for the loss and capture of single electrons by Ar^{40} ions are interpreted by simple statistical arguments.

THE average charge carried by an ion moving through matter depends upon the atomic number z of the ion, the ion's velocity, and the absorbing material. For velocities much greater than the K-electron velocity, i.e., $\beta \gg \beta_K = z/137$, the ion is fully stripped of its electrons. For velocities $\beta \leqslant \beta_K$, the ion is only partially stripped, losing and capturing electrons as it traverses matter. Thus, a beam of ions, after traversing a sufficient amount of homogeneous material, reaches an equilibrium charge distribution that is characteristic of the material, the ion's nuclear charge, and velocity. This paper reports measurements of: (a) the equilibrium distributions of electronic-charge states of C^{12}, N^{14}, O^{16}, and Ne^{20} ions in Zapon at energies between 1.59 and 10.5 MeV/nucleon ($0.0582 \leqslant \beta \leqslant 0.148$), and (b) the nonequilibrium charge distributions for argon ions in Zapon at 10.2 MeV/nucleon ($\beta = 0.146$).

Charge distributions for 0.2- to 1000-keV protons and α particles in gases and solids have been extensively studied. Allison has reviewed the experimental data for these ions.[1] Considerably less information is available for ions heavier than helium, particularly for energies greater than 2.0 MeV/nucleon. Several investigators have measured the equilibrium charge distributions of ions with $z=3$ through $z=10$ in the energy region 0.064 to 2.0 MeV/nucleon in gases and in metallic and organic foils.[2-9] Recently, Nikolaev *et al.* have reported equilibrium charge distributions for several ions with $10 < z < 18$ and for krypton.[10,11] In the energy region below 2.0 MeV/nucleon, nonequilibrium charge distributions were obtained for nitrogen ions in Zapon foils by Reynolds, Wyly, and Zucker,[12] for oxygen ions in argon by Hubbard and Lauer,[2] and for several ions in a variety of gases by Nikolaev *et al.*[13,14] The only measurements within the energy region considered by this paper have been those by Northcliffe who examined the equilibrium charge distributions of energetic O^{16} ions in aluminum foil.[15]

EXPERIMENTAL PROCEDURE

Arrangement

The experimental arrangement is schematically shown in Fig. 1. The ions emerged from the Berkeley heavy-ion linear accelerator (Hilac) with an energy of about 10.2 MeV/nucleon. The ions were degraded to the desired energy by aluminum foils. The first magnet together with the three slits shown produced a well-collimated beam with a momentum spread of about 0.5% at the equilibrium foil. After traversing the equilibrium foil, the ions were separated according to charge by a 22-in.-diam. magnetic spectrometer. The entire beam (now separated into different charge states) was recorded on a single 1.5 in.×18 in. acetate-backed emulsion strip (Ilford, type C.2) placed on the perimeter of the magnet. The ions entered normal to the emulsion surface. The correct exposure times for the emulsions were determined from the counting rates of the counter when the magnetic spectrometer was at zero field.

* Work done under the auspices of the U. S. Atomic Energy Commission.

[1] S. K. Allison, Rev. Mod. Phys. **30**, 1137 (1958).
[2] E. L. Hubbard and E. J. Lauer, Phys. Rev. **98**, 1814 (1955).
[3] V. S. Nikolaev, L. N. Fateeva, I. S. Dmitriev, and Ya. A. Teplova, Soviet Phys.—JETP **5**, 789 (1957).
[4] Ya. A. Teplova, I. S. Dmitriev, V. S. Nikolaev, and L. N. Fateeva, Soviet Phys.—JETP **5**, 797 (1957).
[5] V. S. Nikolaev, I. S. Dmitriev, L. N. Fateeva, and Ya. A. Teplova, Soviet Phys.—JETP **6**, 1019 (1958).
[6] K. G. Stephens and D. Walker, Phil. Mag. **46**, 563 (1955).
[7] K. G. Stephens and D. Walker, Phil. Mag. **45**, 543 (1954).
[8] K. G. Stephens and D. Walker, Proc. Roy. Soc. (London) **A229**, 376 (1955).
[9] H. L. Reynolds, L. D. Wyly, and A. Zucker, Phys. Rev. **98**, 474 (1955).
[10] V. S. Nikolaev, I. S. Dmitriev, L. N. Fateeva, and Ya. A. Teplova, Soviet Phys.—JETP **12**, 627 (1961).
[11] I. S. Dmitriev, V. S. Nikolaev, L. N. Fateeva, and Ya. A. Teplova, Bull. Acad. Sci. U. S. S. R. Phys. Ser. **24**, 1169 (1960).
[12] H. L. Reynolds, L. D. Wyly, and A. Zucker, Phys. Rev. **98**, 1825 (1955).
[13] V. S. Nikolaev, L. N. Fateeva, I. S. Dmitriev, and Ya. A. Teplova, Soviet Phys.—JETP **6**, 239 (1958).
[14] V. S. Nikolaev, I. S. Dmitriev, L. N. Fateeva, and Ya. A. Teplova, Soviet Phys.—JETP **13**, 695 (1961).
[15] L. C. Northcliffe, Phys. Rev. **120**, 1744 (1960).

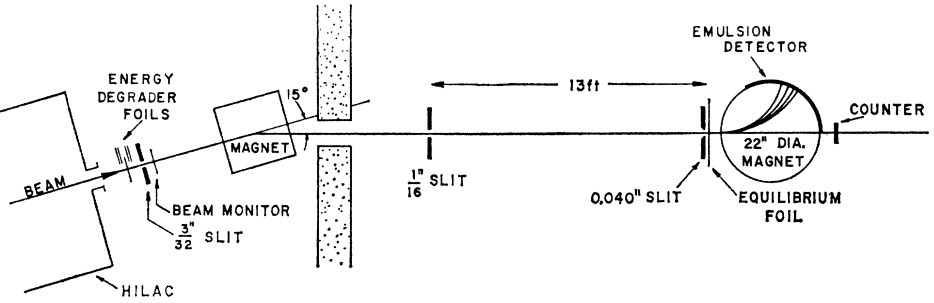

FIG. 1. Schematic diagram of experimental arrangement.

Energy Measurements

The energy, and hence velocity, of the beam was determined from range measurements in 1 in.×3 in. glass-backed 50-μ Ilford C.2 emulsions. As were the film strips, these emulsions were placed on the perimeter of the magnetic spectrometer, but inclined so that the beam entered the emulsion surfaces at a dip angle of 10°. The ranges of the particle tracks were measured with a calibrated eyepiece reticle. The heavy-ion range-energy relations from Heckman *et al.*[16] were used to evaluate beam energies. Corrections for emulsion density and finite grain size (i.e., end corrections) were applied to the measured ranges. For each calibration run, the mean range of about 20 tracks gave a measurement of the ion's velocity β to a statistical accuracy better than 0.2%.

Assurance of Charge-State Equilibrium in Zapon Foil

Charge-state distributions were established in Zapon foils of thicknesses between 20 and 157 μg/cm^2. For all ions except argon, equilibrium charge-state distributions of the ions were obtained for foil thicknesses greater than 50 μg/cm^2. The equilibrium charge-state distributions for carbon, nitrogen, oxygen, and neon ions that are reported are those obtained with Zapon foils 80, 132, and 157 μg/cm^2 thick. Most of the distributions were obtained with the 132-μg/cm^2 foil.

The problem of oil (from the vacuum system) and other foreign matter settling on the equilibrium foil and altering the charge distribution is discussed in reference 1. We have measured the charge distribution from Zapon foils under a variety of changing conditions—e.g., varying the time a foil remained in the vacuum, reversing and stacking foils, varying the age of foils—and have found no significant changes.

We also examined the effect upon the charge distribution of the residual gas atoms in the vacuum system (owing to outgassing of emulsions, particularly). If an ion charge while traversing the magnetic field in route between the foil and detector, a distance of approximately 50 cm, it would appear as a background track between charge-state peaks. The observed spatial distribution of background tracks between the charge-state peaks was compared with the calculated distribution for tracks arising from postfoil charge exchanges. If all background tracks were attributed to postfoil charge exchanges, the calculated corrections to the population number of each charge state would remain less than the statistical errors. To summarize, then, no evidence for systematic errors was found that could significantly alter the charge distributions as observed at the detector. For this reason no such corrections were applied to the experimental data and all quoted errors involve estimates of statistical accuracy only.

The Zapon foils were made by floating thin films of a Zapon solution on water, transferring them to 1-in.-i.d. support rings, and drying them. The foils were removed from the support rings and weighed upon completion of the experiment. Weighing errors were on the order of ± 1 μg/cm^2, an error small in comparison with possible errors that may be introduced through nonuniformity of the foil, dust, and the assumption that 100% of the foil was removed from the mounting ring for weighing. The relative importance of these sources of error was not determined, but the comparison of the data from different foils indicates that the uncertainty in the areal density of the foils is about $\pm 10\%$.

Scanning

The total number of ions in each charge group was determined by visually counting the number of tracks in sample areas of the group. The emulsion technique afforded the advantage that the entire beam divided into charge groups could be detected simultaneously. There was no problem of monitoring the beam, other than estimating the correct exposure, and each ion was detected with 100% efficiency independent of charge, focusing properties of the magnet, etc. Also, an extreme degree of sensitivity could be achieved by exposing several emulsion strips to increasing beam intensities and normalizing the charge distributions observed in each though a common charge state. In this manner it was possible to measure charge states that comprise less than 10^{-5} of the total beam. Figure 2 is a typical film strip in which the profiles of the charge groups $z=18$ through $z=15$ for argon ions are visible. This particular charge distribution was established by a beam of charge-16 argon ions at $\beta=0.146$ after passing

[16] H. H. Heckman, B. L. Perkins, W. G. Simon, F. M. Smith, and W. H. Barkas, Phys. Rev. **117**, 544 (1960).

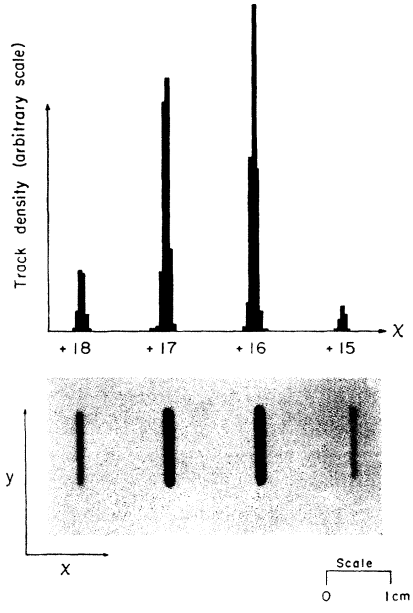

FIG. 2. Film strip in which magnetically separated charge groups Ar^{+18} through Ar^{+15} are evident. The measured profile distributions are shown above the film strip. $\beta=0.146$; 50 $\mu g/cm^2$ Zapon foil.

through a 50-$\mu g/cm^2$ Zapon foil. The measured distribution is shown for comparison.

The method for estimating the total number of tracks in each charge group was as follows: The x profile of each charge group was measured and the standard deviation σ of the distribution was determined. The number of tracks in the charge group was obtained by integrating the areal density of tracks, $(\Delta N_i)/(\Delta y_i)$, observed between $x_0+4\sigma$ and $x_0-4\sigma$ in the increment Δy_i. The increment Δy_i and the spacing of the counted areas were adjusted to give the desired statistical accuracy. Tracks outside the interval $x_0\pm 4\sigma$ were used to estimate the number of background tracks in the charge peaks arising from degraded beam particles, slit scattering, large-angle scattering in the foil, etc.

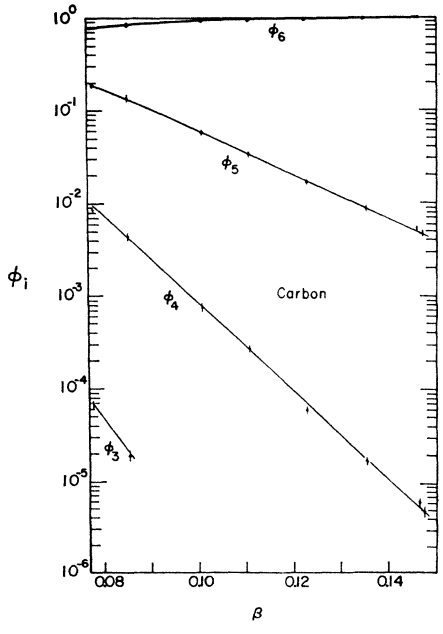

FIG. 3. Equilibrium charge-state distributions for carbon as a function of velocity. The ordinate φ_i is the fraction of ions with charge i. The solid curves superimposed on the data points are calculated from Eq. (2) using the empirical functions M_1, M_2, and M_3.

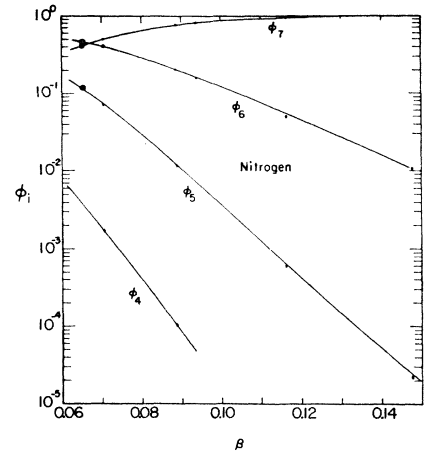

FIG. 4. Equilibrium charge-state distributions for nitrogen as a function of velocity.

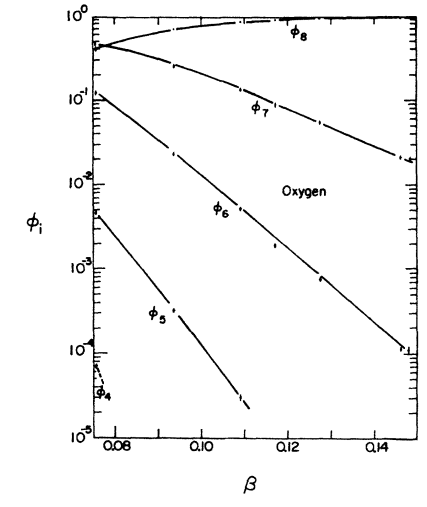

FIG. 5. Equilibrium charge-state distributions for oxygen as a function of velocity.

Corrections for background were usually less than 1%, but in a few instances in which the ion velocity was low and the charge-state fraction was near the threshold for detection the corrections were as high as 10%.

TABLE I. Equilibrium charge-state distributions.

Ion	β	Charge state	φ_i	σ_i
Carbon	0.1477	6	9.953×10^{-1}	1.4×10^{-4}
		5	4.69×10^{-3}	1.4×10^{-4}
		4	4.55×10^{-6}	4.4×10^{-7}
	0.1467	6	9.947×10^{-1}	1.3×10^{-4}
		5	5.31×10^{-3}	1.3×10^{-4}
		4	5.75×10^{-6}	5.6×10^{-7}
	0.1358	6	9.914×10^{-1}	2.3×10^{-4}
		5	8.62×10^{-3}	2.2×10^{-4}
		4	1.60×10^{-5}	1.2×10^{-6}
	0.1231	6	9.828×10^{-1}	4.4×10^{-4}
		5	1.71×10^{-2}	4.3×10^{-4}
		4	5.69×10^{-5}	4.3×10^{-6}
	0.1105	6	9.656×10^{-1}	6.5×10^{-4}
		5	3.41×10^{-2}	6.5×10^{-4}
		4	2.60×10^{-4}	1.1×10^{-5}
	0.1010	6	9.416×10^{-1}	1.25×10^{-3}
		5	5.77×10^{-2}	1.30×10^{-3}
		4	7.38×10^{-4}	2.8×10^{-5}
	0.0854	6	8.590×10^{-1}	2.4×10^{-3}
		5	1.365×10^{-1}	2.4×10^{-3}
		4	4.52×10^{-3}	1.5×10^{-4}
		3	1.9×10^{-5}	1.9×10^{-6}
	0.0780	6	8.009×10^{-1}	2.5×10^{-3}
		5	1.906×10^{-1}	2.5×10^{-3}
		4	8.45×10^{-3}	1.7×10^{-4}
		3	6.65×10^{-5}	2.5×10^{-6}
Nitrogen	0.1475	7	9.895×10^{-1}	2.2×10^{-4}
		6	1.05×10^{-2}	2.1×10^{-4}
		5	2.19×10^{-5}	1.2×10^{-6}
	0.1162	7	9.500×10^{-1}	6.9×10^{-4}
		6	4.94×10^{-2}	6.9×10^{-4}
		5	5.86×10^{-4}	3.4×10^{-5}
	0.0936	7	8.312×10^{-1}	1.5×10^{-3}
		6	1.616×10^{-1}	1.5×10^{-3}
		5	7.19×10^{-3}	1.4×10^{-4}
	0.0888	7	7.831×10^{-1}	2.1×10^{-3}
		6	2.049×10^{-1}	2.1×10^{-3}
		5	1.19×10^{-2}	2.4×10^{-4}
		4	1.05×10^{-4}	3.6×10^{-6}
	0.0704	7	5.078×10^{-1}	2.6×10^{-3}
		6	4.187×10^{-1}	2.6×10^{-3}
		5	7.18×10^{-2}	1.0×10^{-3}
		4	1.74×10^{-3}	3.2×10^{-5}
Oxygen	0.1481	8	9.791×10^{-1}	5.9×10^{-4}
		7	2.04×10^{-2}	5.9×10^{-4}
		6	1.14×10^{-4}	7.7×10^{-6}
	0.1459	8	9.786×10^{-1}	5.0×10^{-4}
		7	2.13×10^{-2}	5.1×10^{-4}
		6	1.17×10^{-4}	4.4×10^{-6}
	0.1273	8	9.435×10^{-1}	1.2×10^{-3}
		7	5.57×10^{-2}	1.2×10^{-3}
		6	7.88×10^{-4}	5.2×10^{-5}
	0.1170	8	9.070×10^{-1}	2.0×10^{-3}
		7	9.10×10^{-2}	2.5×10^{-3}
		6	1.98×10^{-4}	8.1×10^{-5}
	0.1089	8	8.605×10^{-1}	2.2×10^{-3}
		7	1.343×10^{-1}	2.2×10^{-3}
		6	5.20×10^{-3}	1.6×10^{-4}
		5	3.04×10^{-5}	1.5×10^{-6}
	0.0935	8	7.182×10^{-1}	5.0×10^{-3}
		7	2.589×10^{-1}	4.7×10^{-3}
		6	2.26×10^{-2}	7.6×10^{-4}
		5	3.24×10^{-4}	1.2×10^{-5}
	0.0757	8	4.081×10^{-1}	8.6×10^{-3}
		7	4.650×10^{-1}	7.4×10^{-3}
		6	1.222×10^{-1}	2.8×10^{-3}
		5	4.64×10^{-3}	1.3×10^{-4}
		4	7.0×10^{-5}	4.4×10^{-6}
Neon	0.1475	10	9.445×10^{-1}	1.1×10^{-3}
		9	5.47×10^{-2}	1.1×10^{-3}
		8	8.36×10^{-4}	5.3×10^{-5}
	0.1466	10	9.403×10^{-1}	1.9×10^{-3}
		9	5.87×10^{-2}	1.7×10^{-3}
		8	9.91×10^{-4}	4.5×10^{-5}
	0.1205	10	8.209×10^{-1}	3.7×10^{-3}
		9	1.702×10^{-1}	2.9×10^{-3}
		8	8.80×10^{-3}	2.5×10^{-4}
		7	9.81×10^{-5}	7.2×10^{-6}
	0.1101	10	7.170×10^{-1}	4.0×10^{-3}
		9	2.606×10^{-1}	3.9×10^{-3}
		8	2.19×10^{-2}	4.6×10^{-4}
		7	4.25×10^{-4}	1.5×10^{-5}
	0.1014	10	6.073×10^{-1}	4.1×10^{-3}
		9	3.443×10^{-1}	3.7×10^{-3}
		8	4.71×10^{-2}	8.9×10^{-4}
		7	1.35×10^{-3}	4.2×10^{-5}
		6	1.91×10^{-5}	6.8×10^{-7}
	0.0875	10	3.803×10^{-1}	5.7×10^{-3}
		9	4.720×10^{-1}	5.8×10^{-3}
		8	1.395×10^{-1}	2.7×10^{-3}
		7	7.96×10^{-3}	2.1×10^{-4}
		6	1.90×10^{-4}	1.1×10^{-5}
	0.0582	10	3.81×10^{-2}	2.4×10^{-3}
		9	2.958×10^{-1}	6.2×10^{-3}
		8	4.812×10^{-1}	6.7×10^{-3}
		7	1.693×10^{-1}	4.5×10^{-3}
		6	1.56×10^{-2}	7.0×10^{-4}

EQUILIBRIUM CHARGE DISTRIBUTIONS

Results

The experimental results for the equilibrium charge-state distribution of C^{12}, N^{14}, O^{16}, and Ne^{20} ions are summarized in Table I. Tabulated quantities for each ion are its velocity, the charge, the fraction φ_i of the total beam in charge state i at equilibrium, and the statistical standard error σ_i in φ_i. Figures 3 through 6 show the equilibrium charge-state distributions as a function of the ions' velocity β.

Discussion

The theoretical problem of treating the penetration of heavy ions through matter is formidable, and only partial success has been achieved. The discovery of fission gave impetus to theoretical investigations pertaining to ionization processes of the highly charged fission fragments in matter. Bohr,[17–19] Lamb,[20] Knipp and Teller,[21] and Brunings, Knipp, and Teller[22] were among the first authors to examine theoretically the range and effective charge of heavy ions in gases. The more recent theoretical investigations of the capture

[17] N. Bohr, Phys. Rev. **58**, 654 (1940).
[18] N. Bohr, Phys. Rev. **59**, 270 (1941).
[19] N. Bohr, Kgl. Danske Videnskab. Selskab, Mat.-Fys. Medd. **18**, No. 8 (1948).
[20] W. E. Lamb, Jr., Phys. Rev. **58**, 696 (1940).
[21] J. K. Knipp and E. Teller, Phys. Rev. **59**, 659 (1941).
[22] J. M. H. Brunings, J. K. Knipp, and E. Teller, Phys. Rev. **60**, 657 (1941).

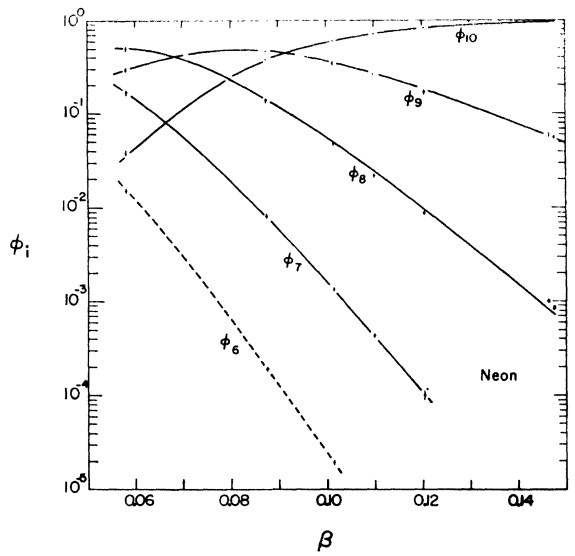

FIG. 6. Equilibrium charge-state distributions for neon as a function of velocity. The dashed curve is not calculated, but serves to connect the experimental points for φ_6.

and loss of electrons by fission fragments and heavy ions in gases have been carried out by Bell,[23] Bohr and Lindhard,[24] and Gluckstern.[25] In most of these efforts the electrons of the charged ions have been described by the Fermi-Thomas model. The differences in each treatment of this complicated phenomenon stem from the various assumptions and mathematical approximations used by the authors in developing their theories. Except for a qualitative discussion of the electron-capture and -loss process in solid materials by Bohr and Lindhard,[24] the theories are limited to rarefied gas strippers—in which the time between successive electron-exchanging collisions is greater than the characteristic lifetimes of the excited states of the ion—and are not directly applicable to this experiment.

Our analysis takes as a basis the phenomenological theory proposed by Dmitriev.[26] A leading assumption in Dmitriev's theory is that the probability for the capture (or loss) of a given electron depends upon the ion's velocity β and is *independent of the capture or loss of the other electrons by the ion.* With this assumption it is possible to express the equilibrium charge fractions φ_i, at velocity β, for an N-electron system in terms of a set of N independent functions, $M_n(\beta)$. The quantity $M_n(\beta)$ is equivalent to an occupation probability, i.e., the probability for finding the nth electron in the ion, while $P_n=1-M_n$ is the probability that the nth electron is absent from the ion. The equilibrium charge distribution φ_i is obtained by summing the fractions of the ions with charge i for the different fixed configurations of the electrons.

[23] G. I. Bell, Phys. Rev. **90**, 548 (1953).
[24] N. Bohr and J. Lindhard, Kgl. Danske Videnskab. Selskab, Mat.-Fys. Medd. **28**, No. 7 (1954).
[25] R. L. Gluckstern, Phys. Rev. **98**, 1817 (1955).
[26] I. S. Dmitriev, Soviet Phys.—JETP **5**, 473 (1957).

For a one-electron system—i.e., a hydrogen ion at a velocity greater than the velocity at which negative-ion formation is important—the charge distribution is simply

$$\varphi_1=P_1, \quad \varphi_0=M_1=1-P_1. \tag{1}$$

The expressions for φ_i for a three-electron system are

$$\begin{aligned}
\varphi_z&=P_1P_2P_3,\\
\varphi_{z-1}&=P_1P_2M_3+P_1P_3M_2+P_2P_3M_1,\\
\varphi_{z-2}&=P_1M_2M_3+P_2M_1M_3+P_3M_1M_2,\\
\varphi_{z-3}&=M_1M_2M_3.
\end{aligned} \tag{2}$$

Specifically, M_1, M_2, and M_3 refer, respectively, to the occupation probabilities for the first, second, and third electron in the ion; φ_z is the observed fraction of totally stripped ions; φ_{z-1} is the fraction of ions that carry one electron, etc. Because most of our measurements are limited to the four highest charge states of the various ions, i.e., a three-electron system, the expressions for φ_i given in Eq. (2) are the ones we actually used to analyze the data. The probabilities M_n that correspond to a given set of observed $\varphi_i(\beta)$ are obtained by solving Eq. (2) for them. The values of M_1, M_2, and M_3 are found to be the roots of a third-order polynomial whose coefficients are linear combinations of the φ_i's.

In order to test Dmitriev's proposal, we have adopted the following point of view: Can the quantities φ_i at given velocity be calculated from a set of independent

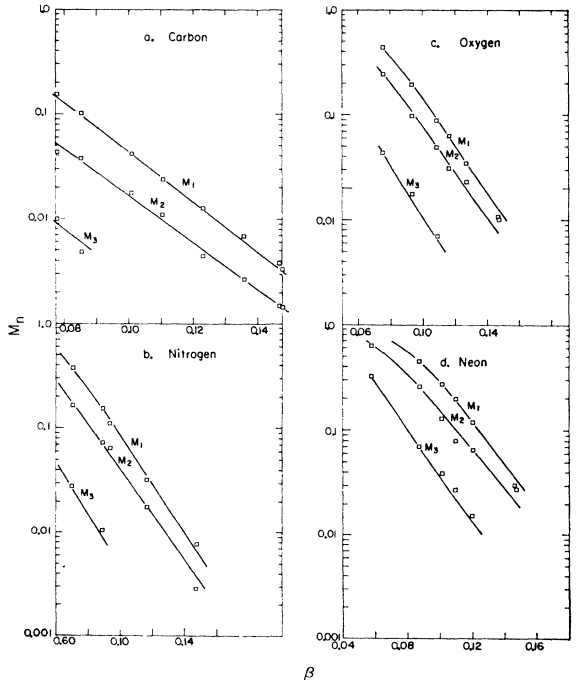

FIG. 7. Occupation probabilities M_n as a function of ion velocity. The curves drawn through the data points are empirical functions of the type given by Eq. (3). The constants chosen to fit the data are listed in Table II.

TABLE II. Constants m, k, and ln$a$ used to fit $M_n(\beta)$ data to Eq. (3).

Ion	M_n	m	k	ln$a$
Carbon	M_1	0.85	48	−3.67
	M_2	0.85	44	−2.00
	M_3	0.85	46	+0.28
Nitrogen	M_1	0.775	45	−5.20
	M_2	0.775	41	−3.70
	M_3	0.775	43	−1.74
Oxygen	M_1	0.70	42	−6.60
	M_2	0.70	38	−5.10
	M_3	0.70	40	−3.42
Neon	M_1	0.55	36	−9.24
	M_2	0.55	32	−7.32
	M_3	0.55	34	−6.31

occupation probabilities M_n? As we shall show, the values of M_n deduced from the data can be well approximated by empirical functions of β from which the equilibrium charge distributions can be calculated.

Figure 7 presents the roots M_1, M_2, and M_3 plotted as a function of velocity for C^{12}, N^{14}, O^{16}, and Ne^{20} ions. All roots are real quantities except for the highest velocity points ($\beta \approx 0.146$) for O^{16} and Ne^{20}. In these cases, the roots have small imaginary parts which are not statistically significant. For all ions it is clearly evident that the roots M_1, M_2, and M_3 generate continuous, monotonically decreasing functions of velocity.

In order to select the form of an empirical function to represent the functions $M_n(\beta)$, we referred to the equilibrium charge distributions of hydrogen ions in various gases and solids.[1] In general, the fraction of the neutral charge component $\varphi_0 \approx M_1$ is well described by a function of the type

$$M_1 = (1+a)/[1+a(\exp k\beta^m)], \qquad (3)$$

where a, k, and m are constants and β is the ion velocity. Assuming that this functional form is valid for all

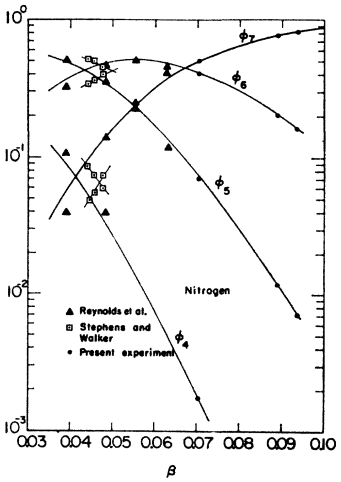

FIG. 8. Calculated charge-state distributions for nitrogen ions at low velocities.

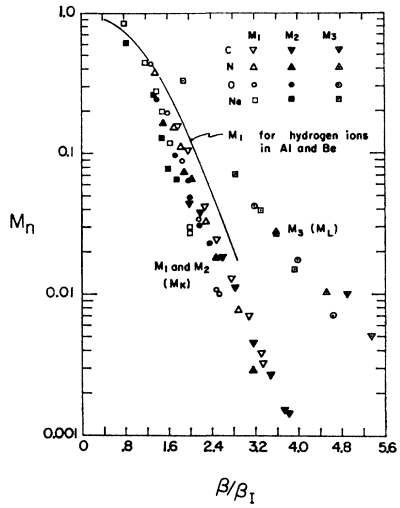

FIG. 9. The occupation probabilities for the K electrons and the first L electron for carbon, nitrogen, oxygen, and neon plotted as a function of β/β_I, where $\beta_I = (2I/m)^{1/2}$. Also shown is the occupation probability M_1 for hydrogen ions in light metals.

$M_n(\beta)$, we adjusted the constants a, k, and m to fit the data points shown in Fig. 7. The charge distributions of hydrogen produced by aluminum and beryllium foils indicated that the exponent m is about 1. The value of m for each ion was obtained by noting that for high velocities the ratio φ_z/φ_{z-1} asymptotically becomes $[a/(a+1)](\exp k\beta^m)$, from which the values of a, k, and m can be estimated. Table II lists the constants m, k, and ln$a$ used to fit the $M_n(\beta)$ data, Fig. 7. The data are satisfactorily represented by taking m to be a constant for each ion, but varying linearly with atomic number. The values of k and a are adjusted to fit the data. These quantities are found to vary smoothly with the charge state as well as with the atomic number of the ion.

Using the empirical functions for M_1, M_2, and M_3 obtained from Eq. (3) and the parameters given in Table II, we calculated the equilibrium charge-state distributions from Eq. (2). The calculated distributions are the solid-line curves shown in Figs. 3 through 6. In all instances in which they are compared the calculated distributions fit the experimental observations extremely well. In Fig. 8 the calculated charge-state distributions for nitrogen ions are extended to lower velocities to encompass the data of Reynolds *et al.*[9] and Stephens and Walker.[8] The data points of Reynolds *et al.* are satisfactorily represented by the calculated distributions. The measurement by Stephens and Walker can also be brought into agreement with the calculated distribution provided the quoted velocities are reduced by approximately 15%.

It should be mentioned that when the fourth ($2L$) electron in neon was included in the analysis, the M_3 and M_4 roots of the fourth-order polynomial obtained were usually imaginary. To carry out these calculations

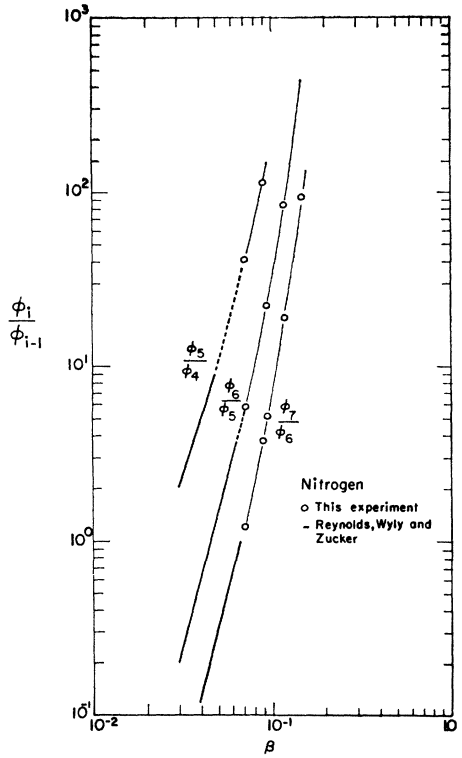

FIG. 10. Ratio of adjacent charge-state fractions for nitrogen ions as a function of velocity. At equilibrium, the ratio ϕ_i/ϕ_{i-1} equals $\sigma_{\text{loss}}/\sigma_{\text{cap}}$, the ratio of loss to capture cross sections for the ith electron.

it was assumed that the occupation probabilities for the fourth, fifth, etc., electron in the ion was negligible relative to M_3. The assumption is likely to be a poor one, since the L-shell occupation probabilities M_3, M_4, $\cdots$ may be, in fact, comparable in magnitude. The reason real roots are obtained when only the probabilities M_1, M_2, and M_3 are considered comes from the observation that the occupation probability for the third ($1L$) electron M_3 is indeed small relative to the K-shell occupation probabilities M_1 and M_2, e.g., $M_3 \approx 0.1 M_2$.

Another assumption Dmitriev proposed for his theory was that the occupation probabilities M, when expressed in the form $M(\beta/\beta_I)$, were the same for all electrons in all atoms. The velocity β_I is taken to be equal to $(2I/m)^{1/2}$, where I is the ionization potential for the given electron. Although we did not assume such a functional form in our analysis described above, we may plot the values of M_n vs β/β_I to examine whether or not such a relation exists. Figure 9 shows that no function of the form $M(\beta/\beta_I)$ can uniquely represent all the data. However, the data do indicate that occupation probabilities for the K electrons, i.e., M_1 and M_2, and the first L electron, M_3, form two sets of loci each of which can be qualitatively represented by $M_K(\beta/\beta_I)$ and $M_L(\beta/\beta_I)$, respectively. The curve of $\varphi_0 \approx M_1$ vs β/β_I for hydrogen ions in aluminum and beryllium foils is also included in the figure. The hydrogen data demonstrate a marked similarity to the heavy-ion data obtained from this experiment. This indicates that for the K electrons, at least, the capture-and-loss mechanism is not strongly dependent upon the atomic number of the ion. The data are insufficient to make such a speculation for the L electrons, but it is clear that the capture-and-loss processes are not alike for the K and L electrons.

Ratios of Loss to Capture Cross Sections

At equilibrium the ratio of adjacent charge-state fractions, φ_i/φ_{i-1}, is equal to the ratio of the loss to capture cross sections for the ith electron:

$$\varphi_i/\varphi_{i-1} = \sigma_{i-1,i}/\sigma_{i,i-1} = \sigma_{\text{loss}}/\sigma_{\text{cap}}. \tag{4}$$

Bohr[19] has estimated that $\sigma_{\text{loss}}/\sigma_{\text{cap}}$ should be proportional to β^r/z^s, where the exponents r and s depend upon the atomic number of the ion and the stopping material. In light stopping materials $r \approx 4$ and $s \approx 7$ for α particles, while for fission fragments Bohr estimated $r \approx 3$ and $s \approx 0$. We find that the velocity exponent r is approximately 5, but varies between 3.6 and 6.6. No definite dependence of r upon the atomic number of the ion is noted. Figure 10 presents the φ_i/φ_{i-1} data for nitrogen ions as a function of β. These data, which are typical for the various ions, are augmented by the low-velocity N^{14} data of Reynolds, Wyly, and Zucker.[9] An extrapolation of the results of our experiment to lower velocities joins smoothly with the data of Reynolds *et al.*

An examination of the dependence of the exponents r and s upon z, i, and β revealed that the ratio s/r is not a constant; hence the ratios φ_i/φ_{i-1} cannot be adequately described by a function of the form of $f(\beta/z^\gamma)$, where $\gamma = s/r$. However, by using an "effective charge" $(i-\alpha)$ instead of z (where i is the charge of the ion and α is an additive constant), we find that the modified function

$$\varphi_i/\varphi_{i-1} = f[137\beta/(i-\alpha)^\gamma]$$

is sufficient to reduce all our experimental data to three universal curves—one each for the $1K$, $2K$, and $1L$ electrons. The values of α and γ that give a best fit to the data are 0.62 and 0.70, respectively. Figure 11 exhibits the results of this analysis. Included in the figure are the ratios of loss to capture cross sections, i.e., φ_i/φ_{i-1}, for the $1K$, $2K$, and $1L$ electrons by C^{12}, N^{14}, O^{16}, and Ne^{20} ions in Zapon for the velocity interval $\beta = 0.058$ to 0.147. Also shown are these same ratios for Ar^{40} ions at $\beta = 0.146$, i.e., $137\beta/(i-0.62)^{0.7} \approx 3$.

Mean Ionic Charge

Brunings, Knipp, and Teller calculated the ratio $\bar{z}/z$, the average charge of the ions to the nuclear charge, as a function of the reduced velocity $V_e/z^{2/3}$.[22] The quantity

V_e is the characteristic velocity within the ion of the electrons participating in the capture and loss processes. The mean charges were calculated for two assumptions: (a) V_e is the velocity of the energetically most easily removable electron as determined from the Fermi-Thomas model; and (b) V_e is the velocity of the outermost electron also calculated from the Fermi-Thomas model. These two assumptions represent opposite extremes, and the characteristic velocity should be between these values.

In both cases, the calculated functions of $V_e/z^{2/3}$ are different for different values of z. However, if $\bar{z}/z$ is plotted as a function of V_e/z^{ϵ}, ϵ can be chosen so that a universal function is obtained for all ions. For assumption (a) $\epsilon=0.55$ and for assumption (b) $\epsilon=0.33$.

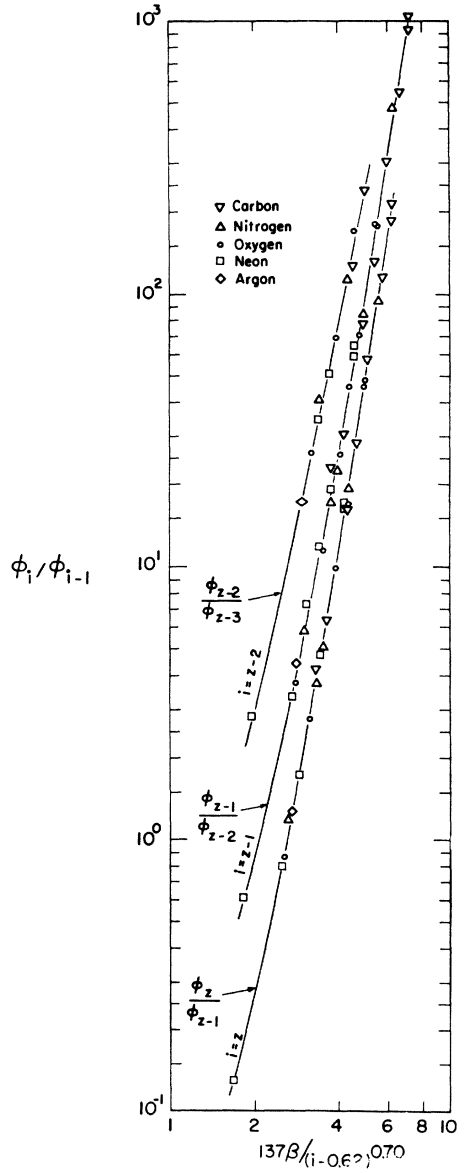

FIG. 11. The ratios ϕ_i/ϕ_{i-1} plotted against $137\beta/(i-0.62)^{0.70}$, where β is the ion's velocity and i is its ionic charge. All equilibrium charge-state data obtained in this experiment are included in the figure.

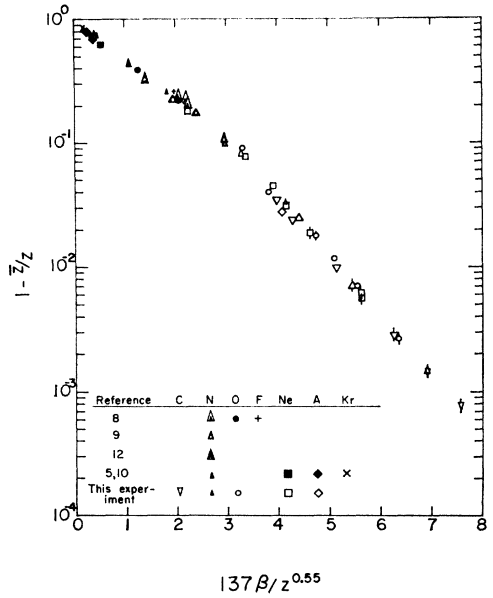

FIG. 12. Measured values of $1-(\bar{z}/z)$vs $\beta/z^{0.55}$. References 8 and 12 and this experiment are in Zapon, reference 9 in Formvar, and references 5 and 10 in celluloid.

If the ratio of V_e to the velocity of the ions βc is the same for all ions, $\bar{z}/z$ will also be a universal function of β/z^{ϵ}. Assuming $\epsilon=2/3$, Papineau used experimental data for nitrogen, oxygen, and neon ions to empirically determine this function.[27] A universal function of this type is very useful for estimating the average charge of ions for which measurements are not available. The data from this experiment give the best universal curve when ϵ is in the region 0.55 to 0.58. A plot of the experimental values of $1-(\bar{z}/z)$ vs β/z^{ϵ} is given in Fig. 12 for $\epsilon=0.55$. Points from other experiments in plastic foils at lower velocities fall close to the same curve, although better agreement with the low-energy data of Nikolaev *et al.* is obtained with a lower value of $\epsilon\approx0.45$.[5,10,11]

NONEQUILIBRIUM CHARGE DISTRIBUTIONS FOR ARGON

When charge distributions for argon ions were obtained, it was discovered that the thickness of the Zapon foils required for equilibrium was about 300 $\mu g/cm^2$. With foils this thick, multiple scattering caused adjacent charge states to overlap except for the highest ion velocity, $\beta=0.146$. However, several nonequilibrium charge distributions were obtained for a beam of Ar^{+16} ions with $\beta=0.146$ incident on the foils. The fraction of the ions in the various charge states for different Zapon foil thicknesses is presented in Table III and is

[27] A. Papineau, Compt. Rend. 242, 2933 (1956).

TABLE III. Nonequilibrium charge-state distributions for Ar^{+16} ions at $\beta=0.146$.

Zapon foil thickness ($\mu g/cm^2$)	φ_{14}	φ_{15}	φ_{16}	φ_{17}	φ_{18}
21	1.55×10^{-3}	5.08×10^{-2}	6.68×10^{-1}	2.51×10^{-1}	2.82×10^{-2}
25	1.60×10^{-3}	5.35×10^{-2}	6.51×10^{-1}	2.62×10^{-1}	3.17×10^{-2}
38	1.44×10^{-3}	4.66×10^{-2}	5.12×10^{-1}	3.62×10^{-1}	7.75×10^{-2}
50	1.23×10^{-3}	3.86×10^{-2}	4.61×10^{-1}	3.98×10^{-1}	1.01×10^{-1}
51	1.0×10^{-3}	3.37×10^{-2}	4.57×10^{-1}	4.07×10^{-1}	1.01×10^{-1}
73	...	2.86×10^{-2}	3.49×10^{-1}	4.69×10^{-1}	1.53×10^{-1}
125	...	1.35×10^{-2}	2.01×10^{-1}	4.80×10^{-1}	3.06×10^{-1}
156	...	9.7×10^{-3}	1.40×10^{-1}	4.59×10^{-1}	3.91×10^{-1}
Equilibrium	...	...	9.10×10^{-2}	4.09×10^{-1}	5.00×10^{-1}
Equilibrium	...	5.1×10^{-3}	8.74×10^{-2}	3.88×10^{-1}	5.19×10^{-1}

plotted in Fig. 13. The errors indicated in Fig. 13 are estimates of the uncertainties in determining the thickness of the foils.

If it is assumed that only one electron is captured or lost in each collision between the ions and the atoms of the foil, the cross sections for capture and loss are given by a set of simultaneous differential equations of the type

$$d\varphi_i/dx=\sigma_{i-1,i}\varphi_{i-1}-(\sigma_{i,i-1}+\sigma_{i,i+1})\varphi_i+\sigma_{i+1,i}\varphi_{i+1}. \quad (5)$$

Here φ_i is the fraction of the ions in the beam with charge i, x is the thickness of the foil that the beam has penetrated, and $\sigma_{j,k}$ is the cross section for a collision in which an ion with charge j changes to an ion with charge k. Assuming various values of the cross sections, we integrated the differential equations numerically and compared the resulting curves of φ_i vs x with the experimental points. The set of cross sections that gave the best fit to the experimental data is given in Table IV. The estimated errors reflect principally the scatter of the data points. The solid lines in Fig. 13 were calculated from these cross sections.

The ratios of the various loss cross sections and of the various capture cross sections in Table IV can be explained with simple statistical arguments if the following assumptions are made: (a) The cross sections for electrons in both K states are about the same. (b) The cross sections for electrons in all L states are nearly equal. (c) As in Dmitriev's theory, the cross sections for an electron in a given state are independent of the occupation of other states by electrons. (d) The time between charge-changing collisions is much less than the time required for radiative transitions between L and K states. Condition (d) is supported by the experimental cross sections. If electrons could readily radiate from the L to the K shell, then one would expect that $\sigma_{18,17}$ is the sum of the capture cross sections into all the L and K states and would thus exceed $\sigma_{16,15}$. This is in disagreement with the experimental values (Table IV).

Under these assumptions the cross section for the loss of one electron by an Ar^{+16} ion carrying two K electrons should be twice the loss cross section for an Ar^{+17} ion carrying one K electron. Similarly, the probability for loss of an electron by an ion carrying two L electrons is twice that for an ion carrying one L electron.

By similar reasoning the cross section for capture of an electron by an Ar^{+16} ion with eight vacant L states should be 8/7 the cross section for capture by an Ar^{+15} ion with seven vacant L states. Ions of Ar^{+17} and Ar^{+18} should capture electrons into an L state with the same cross section as ions of Ar^{+16}. However, as the curve for φ_{15} in Fig. 13 shows, the loss cross section for L

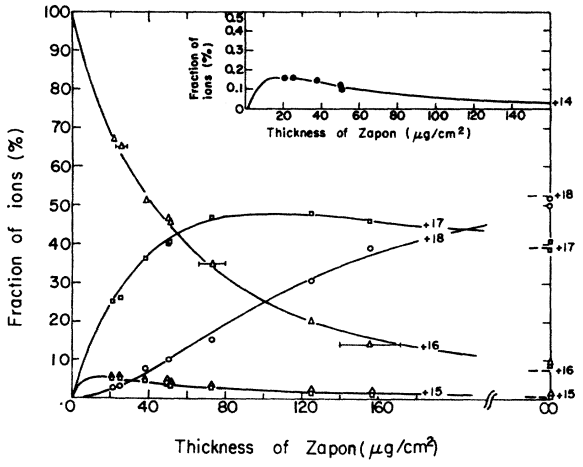

FIG. 13. Nonequilibrium charge-state distributions for argon ions at $\beta=0.146$. The curves are calculated from the set of cross sections given in Table IV.

TABLE IV. Cross sections for loss and capture of a single electron by argon ions at $\beta=0.146$.

	Cross section	$\sigma_{j,k}$ ($cm^2/\mu g$)	$\sigma_{j,k}/\pi a_0^2$ [a]
Loss	$\sigma_{14,15}$	0.36 $\pm$0.09	0.066
	$\sigma_{15,16}$	0.17 $\pm$0.03	0.030
	$\sigma_{16,17}$	0.0165$\pm$0.0005	0.0030
	$\sigma_{17,18}$	0.0090$\pm$0.0005	0.00165
Capture	$\sigma_{15,14}$	0.011 $\pm$0.003	0.0020
	$\sigma_{16,15}$	0.012 $\pm$0.002	0.0022
	$\sigma_{17,16}$	0.0031$\pm$0.0002	0.00057
	$\sigma_{18,17}$	0.0067$\pm$0.0004	0.00114

[a] a_0 is the radius of the first Bohr orbit in the hydrogen atom. To obtain these values, it was assumed that there are 6.2×10^{16} atoms/μg of Zapon.

electrons is so large that the equilibrium between capture and loss of L electrons is established after the ions have penetrated about 10 $\mu g/cm^2$ of the foil. From then on, according to assumptions (c) and (d), the small fraction of the ions that carry L electrons has little effect on the buildup or decay of the fractions of ions with zero, one, and two electrons. Therefore, the experimental values obtained for the cross sections $\sigma_{18,17}$ and $\sigma_{17,16}$ are very nearly the cross sections for capture of K electrons. Since Ar^{+18} ions can capture K electrons into either of the two spin states, $\sigma_{18,17}$ should be twice $\sigma_{17,16}$, which is the cross section for capture into a single K state σ_{cK}.

According to the statistical argument, the cross section of capture into a single L state should be $\sigma_{cL}=\frac{1}{8}\sigma_{16,15}$. The experimental data give $\sigma_{16,15}\approx 4\sigma_{17,16}$. Therefore, $\sigma_{cL}\approx\frac{1}{2}\sigma_{17,16}=\frac{1}{2}\sigma_{cK}$. The ratio σ_{cL}/σ_{cK} thus turns out to be the ratio of the orbital velocities of the first L electron to that of the K electron. This is a weaker dependence on the orbital velocity of the electron in the ion than predicted by the theories of Bohr and Nikolaev,[19,28] but a stronger dependence than given by the theory of Gluckstern.[25]

This statistical picture explains the ratios of the capture cross sections and the loss cross sections obtained for the K electrons of nitrogen ions by Reynolds, Wyly, and Zucker.[12] However, if a similar statistical approach is used to explain the low-energy data of Nikolaev *et al.*,[13] where the nitrogen ions carry many of the L electrons, the agreement is not so good.

Gluckstern estimated that cross sections for capture and loss of two electrons may be an appreciable fraction of the single-electron cross sections.[25] At lower velocities Nikolaev *et al.* found double-capture cross sections as high as 20% of the corresponding single-capture cross sections.[29] Since all the argon ions in our experiment were initially in the +16 charge state, a double-capture cross section $\sigma_{16,14}$ 20% of $\sigma_{15,14}$ would cause considerable error in the value of $\sigma_{15,14}$ given in Table III. However, because, initially, there are no Ar^{+17} or Ar^{+18} ions in the beam, the values of $\sigma_{16,15}$ and $\sigma_{17,16}$ obtained should not be seriously affected by double capture. To make a good determination of whether or not double capture is important, it is necessary to have data for thinner foils (e.g., not more than about 10 $\mu g/cm^2$) where the number of Ar^{+14} and Ar^{+15} ions is still increasing.

ACKNOWLEDGMENTS

The authors wish to give their thanks to Betty L. Perkins for her many contributions to the design and in the carrying out of the experiment. The analysis of the data was done with the able assistance of scientific data analysts Shiela Boehm, Barbara Bole, James Greene, and Charles Jinks. We have benefited greatly from the advice and critical discussions that Walter H. Barkas afforded us throughout this work. We wish to acknowledge the skill of Daniel O'Connel, who made all the Zapon foils for the experiment. Finally, the excellent technical assistance given us by the Hilac operating crew is greatly appreciated.

[28] V. S. Nikolaev, Soviet Phys.—JETP **6**, 417 (1958).

[29] V. S. Nikolaev, L. N. Fateeva, I. S. Dmitriev, and Ya. A. Teplova, Soviet Phys.—JETP **14**, 67 (1962).

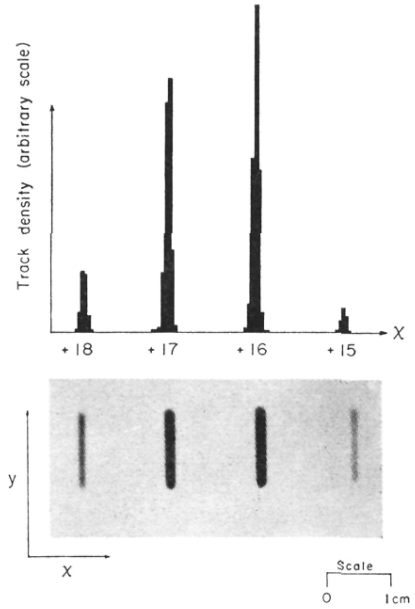

FIG. 2. Film strip in which magnetically separated charge groups Ar^{+18} through Ar^{+15} are evident. The measured profile distributions are shown above the film strip. $\beta \approx 0.146$; 50 $\mu g/cm^2$ Zapon foil.